Behavior of basalt under laser-induced shock-wave application to the planetary hypervelocity impact effect

Laurent Berthe[a)]
Laboratoire PIMM, UPR CNRS 8006/ARTS et METIERS PARIS TECH, 151 Boulevard de l'Hôpital, 75013 Paris, France

Natalia S. Bezaeva
CEREGE, UMR CNRS/Aix-Marseille Université, BP 80, 13545 Aix-en-Provence Cedex 4, France; Department of Earth Science and Engineering, Imperial College London, South Kensington Campus, London SW7 2AZ, United Kingdom; and Earth Physics Department, Faculty of Physics, M.V. Lomonosov Moscow State University, Leninskie gory, 119991 Moscow, Russia

Jerôme Gattaceca
CEREGE, UMR CNRS/Aix-Marseille Université, BP 80, 13545 Aix-en-Provence Cedex 4, France

Michel Boustie and Thibaut de Rességuier
Laboratoire de Combustion et de Détonique, UPR CNRS 9028, ENSMA, 1 Avenue C. Ader, B.P. 40109, 86961 Futuroscope Cedex, France

Pierre Rochette
CEREGE, UMR CNRS/Aix-Marseille Université, BP 80, 13545 Aix-en-Provence Cedex 4, France

(Received 24 June 2008; accepted for publication 25 November 2010; published 10 March 2011)

This paper presents the results of an investigation of the impact of laser-induced shock on basalt samples in a water confinement regime. In order to observe the effect of laser shock-wave propagation, in this material, the rear free surface velocity is measured by a velocimetry interferometer system for any reflector under various specified conditions. Parameters for an elastoplastic constitutive law and the Kanel's damage model are provided and have been set up in such a way to ensure good correlation between numerical simulations and laboratory experiments. These resultant material properties, identified for the basalt sample studied here, could be used in future investigations looking to further correlating residual effects in material with pressure levels induced by water confined laser-matter interaction. This is of particular importance in meteoritics and planetary science due to the fact that hypervelocity impacts represent a major event taking place in the solar system, and shock waves generated during hypervelocity impacts can significantly affect physical properties of extraterrestrial materials and solid solar system bodies such as Mars, the Moon, asteroids, and others. © *2011 Laser Institute of America.*

Key words: Shock, laser, hypervelocity, planetary, magnetization, mechanical properties

I. INTRODUCTION

For investigations of the effects of hypervelocity impacts on the solid solar system bodies (e.g., Earth, Mars, the Moon, etc.), it is essential to know the mechanical behavior of rocks under strong shock waves. For example, the effect of shock waves on the remanent magnetization of basalt can help for better understanding and interpretation of planetary magnetic anomalies observed above impact basins.[1,2] However, the evolution of magnetic properties caused by hypervelocity impacts can be correlated with mechanical effects only if the physical response of basalt under such shock events is well understood.

Compared to widely used plate impact and explosive shock experimental techniques, high-power laser offers an incomparable flexibility allowing an easy recovery of samples (thicker than 3 mm in the present paper) and a wide range of experimental settings (such as a possibility of laboratory shock simulation under a controlled background magnetic field[3]). Besides, a laser can generate a wide range of shock peak pressures from gigapascals[4,5] to terapascals[6,7] with different shock durations,[8] allowing the simulation of loading conditions close to those induced by impacts at a very small scale. By now, very few papers have been published using this promising experimental technique of laser driven shock. Previous results were limited to postmortem analysis of recovered samples. No material properties could be really produced and further investigated.[9]

Some works have been done on mechanical properties of basalt.[10,11] However, they show finally that each rock has proper properties depending on loadings and sources. So, they have to be characterized separately for each source and each loading performed for impact simulations.

This paper presents the evaluation of mechanical properties of a Pleistocene basalt from France (see below) using shock waves, generated by pulsed laser in a water confine-

a)Electronic mail: lberthe@gmail.com

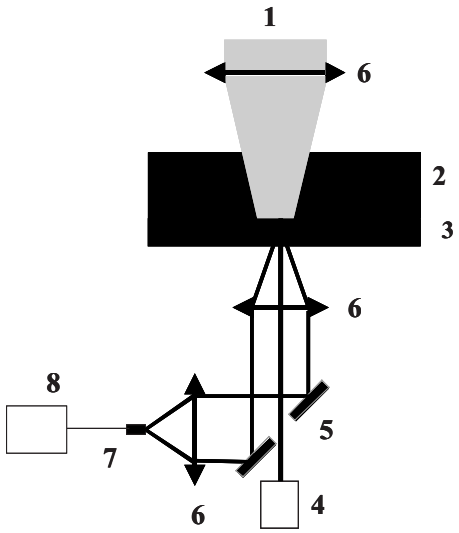

FIG. 1. Experimental setup used for investigations of the behavior of basalt under shock waves, induced by laser in water confinement regime. 1: Laser, 2: water layer for confinement, 3: target, 4: laser probe for rear free surface velocity of target measurement, 5: drilled mirror, 6: lens, 7: fiber, 8: VISAR.

ment regime (WCR).[12] This study proposes the modeling of material in reproducing rear free surface velocity (RFSV) measured by a velocimetry interferometer system for any reflector (VISAR). The first part of the paper presents the experimental setup, and the second part presents a numerical model used to reproduce experimental rear free surface velocities. The last part highlights and discusses the main results.

II. EXPERIMENTAL SETUP

The experimental setup is presented in Fig. 1. It is based on the configuration typical for investigations of shock waves, induced by laser in WCR using a VISAR tool. The numbering on figures corresponds to different parts of the setup.

The laser shock generator from Quantel Company (1) (LCD Facility, Poitiers, France) delivers about 25 J in 20 ns at 1064 nm. The spot diameter is 4 mm, which enables one to ensure a one-dimensional[13] propagation through the target during the acquisition time. The maximum power density is 6 GW cm^{-2}.

The continuous laser probe for RFSV measurements (4) is a VERDI model from Coherent Company working at 532 nm with a maximum power of 5 W to light the rear face of the target (3) covered in front by 1 mm of water. The reflected light from the rear free surface is collected by a lens (6) and a drilled mirror (5) to be focused (6) inside an optical fiber (7) for transfer to the VISAR (8) (from Valyn Company). This tool is based on a Michelson type interferometer[14] and allows velocity measurements from 50 m s^{-1} to several thousands of m s^{-1} with a time precision ranging from 0.5 to 1 ns (according to the velocity range).

The target sample is a Pleistocene basalt from Chanteuges (Haute-Loire, France). Table I provides some information on the properties—parameters of interest for shock-wave propagation. Density and bulk sound velocity values come from direct measurement on the sample;[3] other values, presented in Table I, come from numerical simulations performed to reproduce experimental RFSV. The initial basalt sample is cut using a diamond wire saw into slices (subsamples), whose thickness is between 250 and 3000 μm (unchangeable within each particular subsample). For each target thickness, experiments have been carried out at two power densities: 1.27 ± 0.13 and 5.42 ± 0.85 GW/cm^2. For thickness higher than 2500 μm, targets can be recovered for cross-section analysis using a scanning electron microscope (SEM).

TABLE I. Properties of the target basalt.

General properties	Basalt
Density ρ_0 (kg m^{-3})[a]	3010
Yield strength Y_0 (GPa)[b]	0.200
Shear modulus G (GPa)[b]	23.8
Mie–Grüneisen coefficient γ[b]	2
Bulk sound velocity C_0 (m s^{-1})[a]	5960
Material constant s[b]	−2
Damage model parameters	
Threshold tension (σ_O) (GPa)[b]	0.2
Viscosity constant (k)[b]	2
Critical volume (V_{t1})[b]	0.041

[a]Measured (Ref. 2).
[b]Used to reproduce rear free surface velocity by simulations.

III. SIMULATION TOOLS

A. Models for laser interaction in WCR

Pressure loadings generated by laser in WCR have been calculated according to Refs. 15 and 16. Pressure profiles have been experimentally validated in Ref. 5 with VISAR RFSV measurements.

The maximum pressure, generated by laser plasma in WCR, is given by the following relationship:[15]

$$P(\text{GPa}) = 0.01 \sqrt{\frac{\alpha}{\alpha+3}} \sqrt{Z(\text{g cm}^{-2}\ \text{s}^{-1})} \sqrt{I_0(\text{GW cm}^{-2})}, \quad (1)$$

where α is the fraction of the internal energy devoted to thermal energy (typically α=0.25), I_0 is the incident power density, and Z is the reduced shock impedance between the target and the confining water,

$$2/Z = 1/Z_{\text{water}} + 1/Z_{\text{target}}. \quad (2)$$

For the basalt target in the water confined regime, $Z_{\text{water}} = 0.165 \times 10^6$ g cm^{-2} s^{-1}, $Z_{\text{basalt}} = \rho_0 C_0 = Z_{\text{target}} = 1.8 \times 10^6$ g cm^{-2} s^{-1}, and $Z = 3.04 \times 10^5$ g cm^{-2} s^{-1}.

Figure 2 shows typical pressure loadings used in the SHYLAC software (see below) computation of shock-wave propagation in basalt. The pressure duration (45 ns) is about twice the pulse duration (20 ns) as set up in numerical models. So, the mean pressure peaks, generated for the two experimental power densities (1.27 ± 0.13 and 5.42 ± 0.85 GW/cm^2), are 1.72 and 3.55 GPa, respectively.

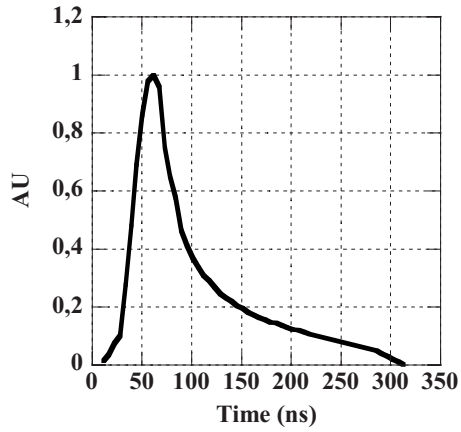

FIG. 2. Typical pressure loadings onto targets used in SHYLAC simulations.

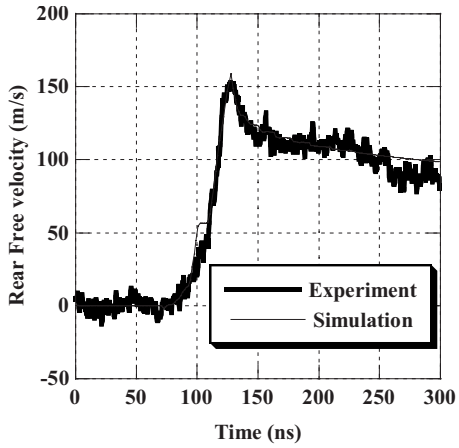

FIG. 3. Typical RFSV for a 500 μm basalt foil at the laser power density of 1.27 ± 0.13 GW/cm^2. Comparison with SHYLAC simulation (peak pressure loading of 1.7 GPa).

B. Propagation of shock waves using SHYLAC software

The SHYLAC software (which is a French abbreviation of "Simulation Hydrodynamique Lagrangienne des Chocs") has been developed at Laboratoire de Combustion et de Détonique, Futuroscope, France for numerical simulations of shock-wave propagation in solids. The physics and computation scheme are detailed in Refs. 17 and 18. SHYLAC is a one-dimensional finite differences code solving the three conservation equations of mass, momentum, and energy.

The Mie–Grüneisen equation of state was used with a reference to the single shock Hugoniot. The Hugoniot is described by the relationship

$$D = C_0 + su, \tag{3}$$

where D is the shock velocity, C_0 is the sound speed at the initial state, s is the dimensionless material constant, and u is the material velocity. This empirical equation is based on experimental shock-wave data first obtained in Ref. 19. An elastic-plastic behavior is included in the code. The axial stress component is calculated as

$$\sigma = -P + 2/3Y_0, \tag{4}$$

where P is the hydrostatic pressure and $2/3Y_0$ is the deviatoric stress (with Y_0 being the yield strength). A standard linear elastic evolution of solid is used in the Von Mises condition to find the elastic/plastic boundary: Strain cannot exceed $Y_0/(2G)$ (where G is the shear modulus) or deviatoric stress cannot exceed $2/3Y_0$.

The dynamic material damage is described with a continuous kinetic criterion, developed by Kanel.[20] The growth of a damage parameter V_t, corresponding to the specific volume of voids inside the target, is calculated by

$$\text{For } |\sigma| > |\sigma_{Oe}|, \quad dV_t/dt = -k \text{ sign}(P)(|\sigma| - \sigma_{Oe})(V_t - V_{t1}), \tag{5}$$

$$\text{For } |\sigma| < |\sigma_{Oe}|, \quad dV_t/dt = 0, \tag{6}$$

$$\text{with } \sigma_{Oe} = \sigma_O(V_{t1}/V_t + V_{t1}). \tag{7}$$

The three parameters in the spallation model mean: σ_O, the threshold tension from which the damage process starts; k, a constant depending on the viscosity related to the strain rate; and V_{t1}, the critical value of V_t from which the growth rate accelerates exponentially.

This model has been extensively developed and validated in the case of spallation induced by laser in Ref. 21. Table I provides the mechanical properties and damage model parameters for basalt target used for SHYLAC simulations.

IV. RESULTS AND DISCUSSIONS

A. Typical RFSV

Figure 3 shows a typical RFSV for a basalt foil at power density of 1.27 ± 0.13 GW/cm^2. It looks like a typical profile for spallation phenomena[22] induced by laser.[4] It can be separated in two parts: a peak of velocity (155 m/s), which is related to the first occurrence of shock wave at the rear surface, and a constant velocity (120 m/s), which corresponds to the flight velocity of the expelled spall. The last part occurs during the decrease of the first peak velocity. Figure 3 also shows a comparison with computer simulations. As seen from Fig. 3, our computation is in good agreement with the experimental profile. However, the elastic precursor breaks ahead of the shock-wave front (as the elastic wave velocity is higher than the plastic wave velocity) on simulation (60 m/s) but not as clearly on the experimental profile.

B. Attenuation as a function of thickness

Figure 4 shows the first peak of RFSV versus the thickness of basalt target for the two power densities. For both intensities, velocity decreases as thickness increases. For 5.42 ± 0.85 GW/cm^2, velocity decreases from 360 to 150 m/s, from 250 to 3000 μm, respectively. For 1.23 ± 0.13 GW/cm^2, velocity drops from 180 to 70 m/s, from 250 to 3000 μm, respectively. Computation using

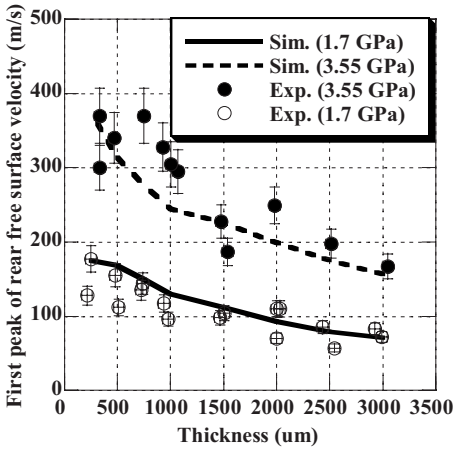

FIG. 4. First peak of RFSV as a function of thickness for basalt at the lowest and highest loadings. Black circle: experiment at 5.42 ± 0.85 GW/cm^2; straight line corresponds to the simulation at peak pressure loading of 3.55 GPa; open circle: experiment at 1.27 ± 0.13 GW/cm^2; dashed line corresponds to the simulation at peak pressure loading of 1.7 GPa.

SHYLAC software is in relatively good agreement with experiments. Consequently, material properties of basalt (Table I) could be used for further investigations aiming to correlate residual effect in material to pressure levels induced in WCR.

C. Material constant *s*

Among properties, a negative material constant s is not conventional [see Table I ($s=-2$)]. It has been already reported, for example, for Vacaville basalt. A negative material constant implies a spreading of the front of shock wave during the propagation inside the material, because bulk sound velocity is lower with high material velocity [see Eq. (3)]. Present results clearly evidence the spreading of the shock front. For instance, Figs. 5(a) and 5(b) present typical RFSVs for basalt targets of 250 and 3000 μm in thickness, respectively, at the highest power density. The rising times of the first velocity peak are 38 and 74 ns at 250 and 3000 μm, respectively. The shock front is well reproduced by simulation, including a negative material constant s.

The validation of this material property can also be confirmed by the shock-wave mean velocity. It depends on shock velocity and material constant s, expressed by Eq. (3). Figure 6 shows this velocity as a function of thickness of the target sample for the two loadings of experiments (1.7 and 3.55 GPa). Curves can be separated in two parts. For the first part, up to 2000 μm, mean velocity increases as a function of thickness (e.g., 2400 m/s at 250 μm and 5000 m/s at 1500 μm for 1.7 GPa loadings). For the second part, starting from 2000 μm and up, mean velocity saturates at the bulk velocity $C_0=5960$ m/s (see Table I). These variations are in agreement with Eq. (3). As the material constant is negative, the shock velocity is clearly below the bulk velocity. When the thickness increases, the material velocity decreases (see Fig. 4) due to the shock attenuation, and so the velocity reaches bulk velocity. Measurements and SHYLAC simulations have a good correlation, which confirms the plausibility of the model used for simulations.

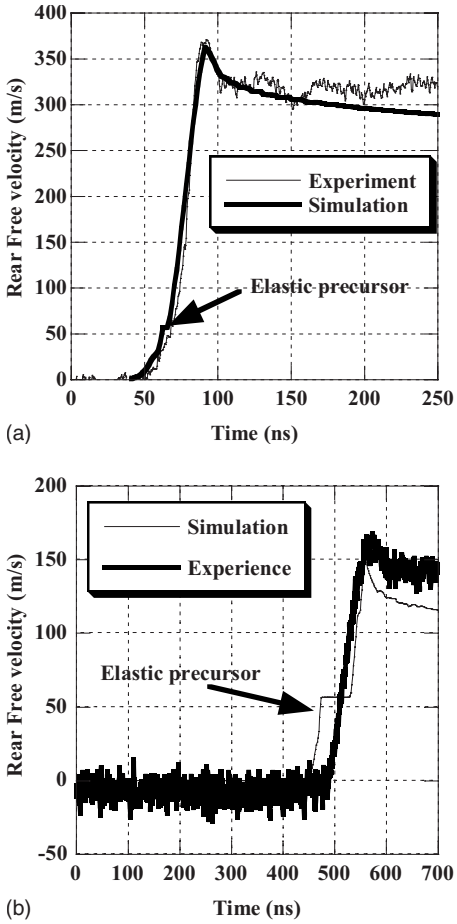

FIG. 5. Typical RFSV at the lowest laser power density of 5.42 ± 0.85 GW/cm^2 for (a) 250 and 3000 μm basalt foils. (b) Comparison with SHYLAC simulations (peak pressure loading of 3.5 GPa).

D. Material heterogeneities

There are some discrepancies between the model and experiments. (1) In Fig. 4, there are some variations between simulations and experiments reaching up to 30% (e.g., for the 750 μm target at the highest power density, SHYLAC gives 280 m/s against 360 m/s for experiment); (2) the

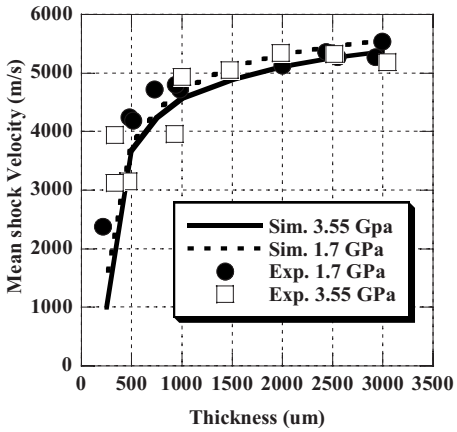

FIG. 6. Mean shock velocity as a function of thickness for high (3.55 GPa) and low (1.7 GPa) loadings. Comparison of laboratory experiments and computer simulations.

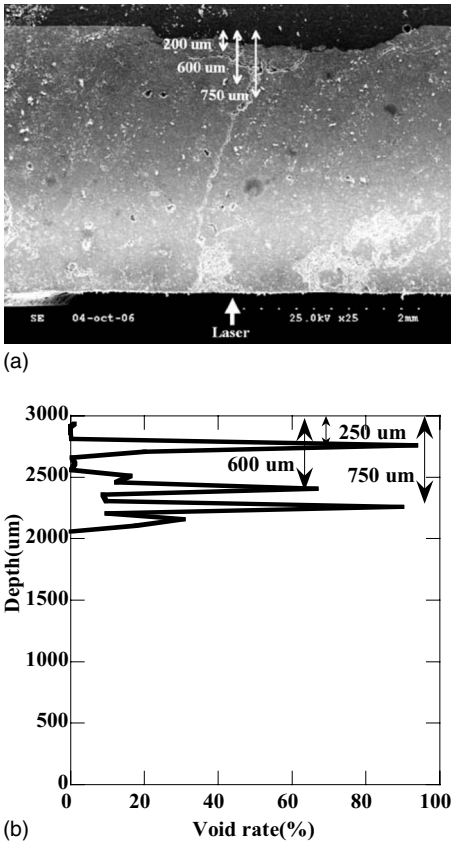

FIG. 7. (a) Image by SEM of a cross section of 3000 μm basalt foil at laser power density of 1.27 ± 0.13 GW/cm^2; (b) corresponding rate of void, calculated using SHYLAC software at time of 700 ns from the irradiation of 1.27 ± 0.13 GW/cm^2 (peak pressure loading: 1.7 GPa). Laser beam comes from bottom (location: 0 μm). Rear free surface is on the top.

elastic precursor ahead of the shock wave does not appear clearly on the experimental profile for thick target [see Figs. 5(a) and 5(b)]. However, for the thickest target [Figs. 5(a) and 5(b)], the elastic precursor is longer than that for the thinnest target. Indeed, it has a velocity lower than the shock-wave one[22] and propagates ahead the shock wave for longer time with thicker target.

These differences could be due to material heterogeneities. Indeed, this basalt has a crystallized matrix with an intergranular texture containing different minerals (e.g., clinopyroxene, plagioclase, olivine, and opaque minerals, among others), whose properties could be very different. This basalt also contains about 5% of phenocrystals (mainly olivine and clinopyroxene in equal proportion, and some rare opaque minerals), which are up to 1.5 mm in size. It is obvious that a numerical model cannot take into account these small-scale heterogeneities.

E. Damage models

SHYLAC predicts the damage location inside the target which can be compared with the experimental one as in Fig. 7. Figure 7(a) shows a SEM image of a recovered sample of 3000 μm irradiated by the lowest power density (1.27 ± 0.13 GW/cm^2). The laser beam comes from the bottom of the sample. Three areas can be observed. The first area is up to 250 μm from the rear free surface. The basalt sample is expelled by the damage process: There is no more material left. The second area is close to 600 μm from the rear surface: A fracture along the surface occurs without any expulsion of material. In the third area, at 700 μm from the rear surface, a deep fracture is generated. It propagates toward the front surface. Figure 7(b) presents the computation of rate of void as a function of thickness for loading, which corresponds to that in Fig. 7(a) (peak pressure loading of 1.7 GPa). Three main void locations are also clearly evidenced at the same location as those observed on cross section in Fig. 7(a): 200, 600, and 750 μm. However, the code does not reproduce the fracture going up to the front surface. Indeed, the propagation of the fracture could be produced at longer time than this simulation (700 ns). It is obvious that a one-dimensional and one damage model is not adapted to treat accurately this case of fractures. To be computed correctly, it necessitates the use of multidimensional models. However, both damage location and RFSV are in agreement with experiments and validate the damage model, used in simulations for the time scale of experiments. For further investigations concerning residual effect, induced by laser shocks, the best way is to use thicker samples to avoid damage processes, induced near the rear free surface.[3]

V. CONCLUSIONS

The behavior of basalt under shock induced by laser in WCR is investigated in detail. Numerical simulations using SHYLAC software reproduce experimental measurements of RFSV for loadings under 6 GPa and initial duration in the range of 50 ns. Under these conditions, the set of parameters for the constitutive elastoplastic law and Hugoniot description evidence the main features of propagation demonstrated by laboratory experiments: a decrease of shock velocity when shock pressure increases, leading to a spreading of compression instead of a stiffening as in most of materials. With these parameters, the decay of the initial loading can be reproduced after propagation within a few millimeters. Concerning the damaging of the basalt upon traction, induced by shock-wave propagation, an average estimate can be provided with Kanel's model for locating coarsely the damaged zone and reproducing the corresponding RFSV. All these data can be used for further works aiming to correlate residual effect in basalt to pressure levels induced by water confined laser-matter.

[1] J. Gattacceca, A. Lamali, P. Rochette, M. Boustie, and L. Berthe, "The effects of explosive-driven shocks on the natural remanent magnetization and the magnetic properties of rocks," Phys. Earth Planet. Inter. **162**, 85–98 (2007).
[2] J. Gattacceca, M. Boustie, B. P. Weiss, P. Rochette, E. Lima, L. E. Fong, and F. Baudenbacher, "Investigating impact demagnetization through laser impacts and SQUID microscopy," Geology **34**, 333–336 (2006).
[3] J. Gattacceca, L. Berthe, T. Boustie, T. Vadeboin, P. Rochette, and T. De Resseguier, "On the efficiency of shock magnetization processes," Phys. Earth Planet. Inter. **166**, 1 (2008).
[4] L. Tollier, R. Fabbro, and E. Bartnicki, "Study of the laser-driven spallation process by the velocity interferometer system for any reflector interferometry technique. I. Laser shock characterization," J. Appl. Phys. **83**, 1224–1230 (1998).

[5]L. Berthe, R. Fabbro, P. Peyre, L. Tollier, and E. Bartnicki, "Shock waves a from water-confined laser-generated plasma," J. Appl. Phys. **82**, 2826–2832 (1997).
[6]R. J. Trainor, J. W. Shaner, J. M. Auerbach, and N. C. Holmes, "Ultrahigh pressure laser-driven shock-wave experiments in aluminum," Phys. Rev. Lett. **42**, 1154–1157 (1979).
[7]R. Cauble, D. W. Phillion, T. J. Hoover, N. C. Holmes, J. D. Kilkenny, and R. W. Lee, "Demonstration of 0.75 Gbar planar shocks in X ray driven colliding foils," Phys. Rev. Lett. **70**, 2102–2105 (1993).
[8]T. de Rességuier, H. He, and P. Berterretche, "Use of laser-accelerated foils for impact study of dynamic material behaviour," Int. J. Impact Eng. **31**, 945–956 (2005).
[9]J. A. Bolger, C. S. Monstross, and A. V. Rode, "Shock wave in basalt rock generated with high powered lasers in confined geometry," J. Appl. Phys. **86**, 5461–5466 (1999).
[10]T. J. Ahrens and M. L. Johnson, *Shock Wave Data for Rocks, Rock Physics and Phase Relations*, Handbook of Physical Constants (American Geophysical Union, Washington, D.C., 1995), pp. 35–43.
[11]S. Nakazawa, S. Watanabe, Y. Iijima, and M. Kato, "Experimental investigation of shock wave attenuation in basalt," Icarus **156**, 539–550 (2002).
[12]N. C. Anderholm, "Laser generated stress wave," Appl. Phys. Lett. **16**, 113–115 (1970).
[13]M. Boustie, J. P. Cuq-Lelandais, C. S. Bolis, S. Barradas, M. Arrigoni, T. de Resseguier, and M. Jeandin, "Study of damage phenomena induced by edge effects into materials under laser driven shocks," J. Phys. D: Appl. Phys. **40**, 7103–7108 (2007).
[14]L. M. Barker and R. E. Hollenbach, "Laser interferometer for measuring high velocities of any reflecting surface," J. Appl. Phys. **43**, 4669–4675 (1972).
[15]R. Fabbro, J. Fournier, P. Ballard, D. Devaux, and J. Virmont, "Physical study of laser-produced plasma in confined geometry," J. Appl. Phys. **68**, 775–784 (1990).
[16]A. Sollier, L. Berthe, B. Bartnicki, P. Peyre, and R. Fabbro, "Study of dense-low temperature plasma generated during laser shock processing of metallic materials in water confined regime," *IFSA Conference* (Elsevier, Kyoto, 2001), pp. 1060–1064.
[17]Y. B. Zel'dovich and Y. P. Raizer, *Physics of Shock Waves and High-Temperature Hydrodynamic Phenomena* (Academic, New York, 1966), Vol. I, pp. 1–96.
[18]F. Cottet and M. Boustie, J. Appl. Phys. **66**, 4067–4073 (1989).
[19]M. H. Rice, R. G. d. Mc Queen, and J. M. Walsh, *Solids State Physics*, edited by F. Steiz and D. Thurnbull (Academic, New York, 1958), Vol. 6, pp. 1–63.
[20]T. Antoun, L. Seaman, D. R. Curan, G. I. Kanel, S. V. Razorenov, and A. V. Utkin, *Spall fracture*," (Springer, New York, 2003).
[21]L. Tollier, R. Fabbro, and E. Bartnicki, "Study of the laser-driven spallation process by the velocity interferometer system for any reflector interferometry technique. II. Experiment and simulation of the spallation process," J. Appl. Phys. **83**, 1231–1237 (1998).
[22]T. Antoun, L. Seaman, D. R. Curan, G. I. Kanel, S. V. Razorenov, and A. V. Utkin, *Spall Fracture* (Springer-Verlag, New York, 2003), pp. 39–55.